

Synchronous Image-Label Diffusion Probability Model with Application to Stroke Lesion Segmentation on Non-contrast CT

Jianhai Zhang¹ Tonghua Wan² Ethan MacDonald¹ Bijoy Menon¹
Aravind Ganesh¹ Qiu Wu²

1. University of Calgary

2. Huazhong University of Science and Technology

Abstract. Stroke lesion volume is a key radiologic measurement for assessing the prognosis of Acute Ischemic Stroke (AIS) patients, which is challenging to be automatically measured on Non-Contrast CT (NCCT) scans. Recent diffusion probabilistic models have shown potentials of being used for image segmentation. In this paper, a novel Synchronous image-label Diffusion Probability Model (SDPM) is proposed for stroke lesion segmentation on NCCT using Markov diffusion process. The proposed SDPM is fully based on a Latent Variable Model (LVM), offering a complete probabilistic elaboration. An additional net-stream, parallel with a noise prediction stream, is introduced to obtain initial noisy label estimates for efficiently inferring the final labels. By optimizing the specified variational boundaries, the trained model can infer multiple label estimates for reference given the input images with noises. The proposed model was assessed on three stroke lesion datasets including one public and two private datasets. Compared to several U-net and transformer based segmentation methods, our proposed SDPM model is able to achieve state-of-the-art performance. The code is publicly available.

Keywords: Diffusion probability model · Medical image segmentation · Coupled Markov stochastic process

1 Introduction

Stroke lesion volume is a key radiologic measurement in assessing prognosis of Acute Ischemic Stroke (AIS) patients [1]. Early assessment of patient outcome is beneficial to inform patients about future perspectives as soon as possible, and to enable treating physician to adapt and personalize the treatments and rehabilitation plans. Ischemic stroke lesions, such as hemorrhagic and ischemic infarct, are typically measured on post treatment Non-Contrast CT (NCCT) scans. Manual contouring of stroke lesions are still clinically deemed as gold standard for volume measurement even though it is time consuming and observer dependent [2,3]. Regardless of many attempts to automate segmentation for

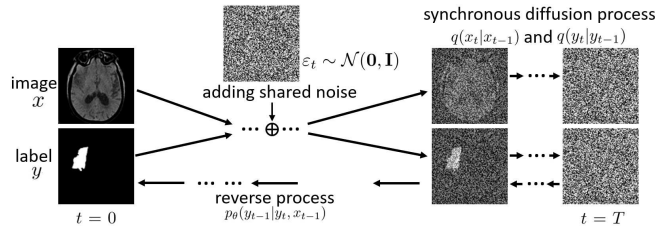


Fig. 1. Synchronous diffusion and reverse processes utilized in our proposed SDPM

stroke lesions [4,5,6], there are still no methods well-established for NCCT, as cerebral CT is limited due to low signal to noise ratio, low contrast of soft tissues, partial volume effects, and acquisition variability across different scanners [7].

This study aims to develop a Diffusion Probabilistic Model (DPM) based approach [8] to accurately segmenting ischemic or hemorrhagic lesion on NCCT. Recently, the methods [9,10,11] based on DPM have received increasing attention for medical image segmentation. The attention is warranted because of the powerful denoising mechanism against even high degrees of noise contamination. In essence, a progressive denoising process [12] for image generation (or potential image labels) is foundationally different from the previous techniques outputting results immediately. Moreover, the introduction of denoising for training indeed improves the robustness of the prediction because of the massive observations with different degrees of noises. Thus, the stability of segmentation performance is able to be guaranteed. Nevertheless, the current diffusion models for medical image segmentation [10,11] are simply treating the image as the conditional input fed to the models without probabilistic interpretability.

In this paper, based on a fully generative Latent Variable Model (LVM), a Synchronous image-label Diffusion Probability Model (SDPM) is proposed for efficiently inferring segmentation labels. To this end, we developed a specified variant of variational inference method and a set of related strategies, including synchronous image-label diffusion process illustrated in Fig.1 and a two-stream network of predicting initial noisy label where the inference process starts, to fit our segmentation task, efficiently restoring the segmentation labels from noisy initials. Accordingly, the label inference methods are implemented in four different ways with their own strength, making SDPM more flexible and applicable. Our contributions briefly include:

1) SDPM is proposed using a synchronous Markov diffusion process for medical image segmentation task. SDPM is based on the fully generative latent variable model with derivational interpretability.

2) A specified variational inference and the involved strategies are proposed for training SDPM. Four inference algorithms in different ways are proposed to efficiently obtain final labels.

2 Methodology

2.1 Revisit diffusion model

As a LVM, diffusion model [8,13] has been successfully applied to the field of image generation with the form $p_\theta(x_0) \triangleq \int p_\theta(x_{0:T}) dx_{1:T}$, where $x_{1:T}$ are the latent variables, x_0 follows an approximately sampled distribution $q(x_0)$. The joint distribution $p_\theta(x_{0:T})$ is called the reverse process [14] modeled by a first-order Markov chain starting at $x_T \sim \mathcal{N}(\mathbf{0}, \mathbf{I})$. The diffusion process $q(x_{1:T}|x_0)$ is also a Markov chain, which adds standard normal noise with a variance schedule β_t . All the mathematical notations are as same as in the paper [13]:

$$p_\theta(x_{0:T}) \triangleq p(x_T) \prod_{t=1}^T p_\theta(x_{t-1}|x_t), \quad q(x_{1:T}|x_0) \triangleq \prod_{t=1}^T q(x_t|x_{t-1}) \quad (1)$$

Minimizing the Kullback-Leibler (KL) Divergence between $q(x_{1:T}|x_0)$ and $p_\theta(x_{0:T})$ will optimize the variational boundary on the negative log-likelihood. To efficiently implement this minimization, two properties are utilized: 1) the observation x_t is sampled at any time in a closed form:

$$q(x_t|x_0) \triangleq \mathcal{N}(x_t|\sqrt{\bar{\alpha}_t}x_0, \gamma_t\mathbf{I}), \quad \bar{\alpha}_t = \prod_{k=1}^t \alpha_k, \alpha_t = 1 - \beta_t, \gamma_t = 1 - \bar{\alpha}_t \quad (2)$$

2) a vicarious posterior $q(x_{t-1}|x_t, x_0)$ with condition x_0 is used for an intractable posterior $q(x_{t-1}|x_t)$ when training the model:

$$q(x_{t-1}|x_t, x_0) \triangleq \mathcal{N}(x_{t-1}|\tilde{\mu}_t(x_t, x_0), \tilde{\beta}_t\mathbf{I})$$

where $\tilde{\mu}_t(x_t, x_0) = \sqrt{\bar{\alpha}_{t-1}}\beta_t\gamma_t^{-1}x_0 + \sqrt{\alpha_t}\gamma_{t-1}\gamma_t^{-1}x_t$ and $\tilde{\beta}_t = \beta_t\gamma_{t-1}\gamma_t^{-1}$ (3)

After simplifying the loss function, the optimization process is equivalent to predict the noise ε_t from the diffused image x_t using a neural network:

$$\mathcal{L} = \mathbb{E}_{x_t, \varepsilon_t \sim \mathcal{N}(\mathbf{0}, \mathbf{I})} [2\sigma_t^2 \alpha_t \beta_t^{-2} \gamma_t \|\varepsilon_t - \hat{\varepsilon}_t(x_t, t)\|^2] \quad (4)$$

The convergent model is capable of inferring the unseen images from the random noise following the standard normal distribution.

2.2 SDPM for Semantic Segmentation

We extend the diffusion model to segmentation tasks with the form $p_\theta(y_0|x_0) = p_\theta(y_0, x_0)/p_\theta(x_0) \propto p_\theta(y_0, x_0)$, where $p_\theta(y_0, x_0) \triangleq \int p_\theta(x_{0:T}, y_{0:T}) dx_{1:T}, y_{1:T}$, and $y_{1:T}$ are new members of latent variables. In the new model, the joint distribution $p_\theta(x_{0:T}, y_{0:T})$ is defined as the reverse process, and it can be factorized as an original DDPM [13] part $p_\theta(x_{0:T})$ and a conditional reverse process $p_\theta(y_{0:T}|x_{0:T})$, which is a series of terms by Markov chains starting at $p_\theta(y_T|x_T)$:

$$p_\theta(y_{0:T}|x_{0:T}) = p_\theta(y_T|x_T) \prod_{t=1}^T p_\theta(y_{t-1}|y_t, x_{t-1}) \quad (5)$$

The diffusion process is an approximate conditional posterior $q(y_{1:T}|y_0, x_{0:T})$:

$$q(y_{1:T}|y_0, x_{0:T}) = \prod_{t=1}^T q(y_t|y_{t-1}, x_t) \quad (6)$$

A KL Divergence is defined between the diffusion process $q(y_{1:T}|y_0, x_{0:T})$ and the reverse process $p_\theta(y_{0:T}|x_{0:T})$ to obtain the variational upper bound on the negative log likelihood because of the non-negative property of KL divergence [15]:

$$\mathbb{KL}(q(y_{1:T}|y_0, x_{0:T})||p_\theta(y_{1:T}|y_0, x_{0:T})) - \mathbb{E}_q[\log p_\theta(y_0|x_0)] \geq 0 \quad (7)$$

The loss function is then defined as minimizing the KL divergence of the conditional posterior and the unnormalized distribution:

$$\begin{aligned} \mathcal{L} &\triangleq \mathbb{E}_q \left[\log \frac{p_\theta(y_0|x_0)}{p_\theta(y_T|x_T)} + \sum_{t=1}^T \log \frac{q(y_t|y_{t-1}, x_t)}{p_\theta(y_{t-1}|y_t, x_{t-1})} - \log p_\theta(y_0|x_0) \right] \\ &= \mathbb{E}_q \left[\log q(y_T|y_0) + \sum_{t=2}^T \log \frac{q(y_{t-1}|y_t, y_0, x_t)}{p_\theta(y_{t-1}|y_t, x_{t-1})} \right] - \log p_\theta(y_0|y_1, x_0) p_\theta(y_T|x_T) \quad (8) \end{aligned}$$

Eq.(8) indicates the acquisition of y_0 could be the traditional way of outputting the label $x_0 \mapsto y_0$, or a generative way of Markov chains by inference $x_T \mapsto y_0$. Namely, as long as an initial label estimate y_T exists, the trained diffusion model can infer back and get the label y_0 . To this end, an additional sub-network for estimating the noisy label y_T from the image x_T is introduced into the network.

Unfortunately, it is difficult to estimate a proper initial y_T for the subsequent inference, because image information is severely destroyed. It is less likely to predict y_T from the image x_T nearly following the distribution $\mathcal{N}(\mathbf{0}, \mathbf{I})$. Thus, $-\log p_\theta(y_T|x_T)$ is a very strong restriction for predicting the initial y_T . Using the final initial y_T could produce a poor result and degrade the segmentation performance notably. To obtain a good initial y_t for inferring y_0 , we add a time window of length T_p to train the model at each time (the loss \mathcal{L}_p in Eq.(9)), guaranteeing that the label y_0 could be efficiently restored. Introducing the prospect to predict an initial y_t , the acquisitions of y_{t-1} do not solely depend on the immediate outputs of the network fed by the noisy image x_{t-1} any longer. The term $\mathbb{E}_q[\log q(y_T|y_0)]$ is constant and thus can be omitted. Therefore, the loss function is further simplified as:

$$\mathcal{L} = \underbrace{\mathbb{E}_q \left[\sum_{t=2}^T \log \frac{q(y_{t-1}|y_t, y_0, x_t)}{p_\theta(y_{t-1}|y_t)} \right]}_{\mathcal{L}_d} - \underbrace{\sum_{t=0}^{T_p} \log p_\theta(y_t|x_t)}_{\mathcal{L}_p} - \underbrace{\log p_\theta(y_0|y_1)}_{\mathcal{L}_{d_0}} \quad (9)$$

For the loss \mathcal{L}_d , the term $p_\theta(y_{t-1}|y_t)$ in reverse process is still compared using KL divergence by the conditional posterior $q(y_{t-1}|y_t, y_0, x_t)$ in the diffusion process introduced in [13]. To make the distribution $q(y_{t-1}|y_t, y_0, x_t)$ tractable, a further assumption is made that images and labels are both overlain by the same

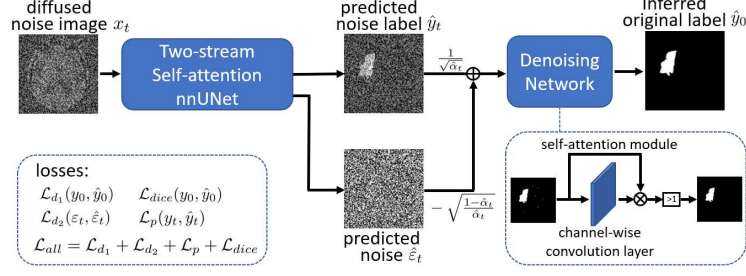


Fig. 2. The training process of the proposed SDPM with the supervised loss functions

Gaussian noise during the diffusion process, i.e., synchronous image-label diffusion process. Thus, the posterior $q(y_{t-1}|y_t, y_0, x_t)$ is degenerated as $q(y_{t-1}|y_0, \varepsilon_t)$, which only relies on the noise at time t and y_0 :

$$q(y_{t-1}|y_0, \varepsilon_t) = \mathcal{N}(y_{t-1}|\tilde{\mu}_t, \tilde{\beta}_t \mathbf{I})$$

where $\tilde{\mu}_t = \sqrt{\bar{\alpha}_{t-1}}y_0 + \sqrt{\alpha_t}(\gamma_{t-1}\gamma_t^{-\frac{1}{2}})\varepsilon_t$, $\tilde{\beta}_t = \beta_t\gamma_{t-1}\gamma_t^{-1}$ (10)

Since the diffusion process for images and labels are shared with the same noise $\varepsilon_t \sim \mathcal{N}(\mathbf{0}, \mathbf{I})$, the images and labels at time t can thus be sampled as:

$$x_t = \sqrt{\bar{\alpha}_t}x_0 + \sqrt{\gamma_t}\varepsilon_t, \quad y_t = \sqrt{\bar{\alpha}_t}y_0 + \sqrt{\gamma_t}\varepsilon_t$$
 (11)

The loss \mathcal{L}_{d_0} is for optimizing the last step of generating y_0 . Some cumbersome discrete segmentation points might degrade the performance to some degree. To refrain from the influence from those points, in addition to applying the same strategy of stopping adding the uncertainty inference of variance $\tilde{\beta}_1$ in [13], we also append a self-attention module with a convolutional layer of frozen parameters of all ones to get rid of the discrete points with a proper threshold, as illustrated in Fig.2.

2.3 Optimizing SDPM

The choice for the transition term $p_\theta(y_{t-1}|y_t)$ in the reverse process is still a Gaussian distribution, i.e., $\mathcal{N}(\mu_\theta(y_t, t), \sigma_t^2 \mathbf{I})$, where θ is the trainable parameters and $\sigma_t^2 = \beta_t$ or $\sigma_t^2 = \tilde{\beta}_t$ are suggested in [13]. The loss \mathcal{L}_d is reparameterized as:

$$\mathcal{L}_d = \mathbb{E}_q \left[\frac{1}{2\sigma_t^2} \|\tilde{\mu}_t(y_0, \varepsilon_t) - \mu_\theta(y_0, \varepsilon_t)\|^2 \right] - \underbrace{2^{-1}D \log \tilde{\beta} + D \log \sigma_t}_C$$
 (12)

where D is image dimensionality. The loss function reveals that as long as the model μ_θ is able to predict $\tilde{\mu}_t$ given the label y_0 with the shared ε_t in the posterior, the final label y_0 is able to be inferred by Markov process.

To further reduce the uncertainty of inferring y_0 through stochastic samplings of $q(y_{t-1}|y_0, \varepsilon_t)$, different from the original DDPM [13], SDPM adds another loss function to restrict the difference between the true and predicted final labels y_0 :

$$\mathcal{L}_d = \mathbb{E}_{y_0, \varepsilon_t \sim \mathcal{N}(\mathbf{0}, \mathbf{I})} \left[\underbrace{\frac{\bar{\alpha}_{t-1}}{2\sigma_t^2} \|y_0 - \hat{y}_0(\hat{y}_t, \hat{\varepsilon}_t, t)\|^2}_{\mathcal{L}_{d_1}} + \underbrace{\frac{\alpha_t \gamma_{t-1}^2}{2\sigma_t^2 \gamma_t} \|\varepsilon_t - \hat{\varepsilon}_t(y_t, t)\|^2}_{\mathcal{L}_{d_2}} \right] + \xi \quad (13)$$

where $\hat{y}_0 = \hat{y}_t / \sqrt{\bar{\alpha}_t} - \sqrt{\gamma_t / \bar{\alpha}_t} \hat{\varepsilon}_t$ and ξ is a binomial residue term. As the losses \mathcal{L}_{d_1} and \mathcal{L}_{d_2} are getting optimized, the ξ is also getting optimized and thus has been ignored for now. Notice that it is impossible to predict ε_t from the label y_t , because there is no image information from y_t at all. Fortunately, from [9,16], the network predicting the noise at each diffusion process also carries the label information. Thus, the model can utilize x_t to predict the shared noise $\hat{\varepsilon}_t(x_t, t)$.

For the loss \mathcal{L}_p , since the network can predict stochastic noise, the noisy labels y_t can thus be predicted with the supervision of the noised label:

$$\mathcal{L}_p = \mathbb{E}_{x_t \sim q(x_t|x_0)} \left[\|y_t - \hat{y}_t(x_t, t)\|^2 \right] \quad (14)$$

To further improve the segmentation performance, a classic dice loss can also be applied to this composite loss function with the treatment of adding an activation function of sigmoid directly at the last layer of outputting y_0 . The supervised loss functions are illustrated in Fig.2.

2.4 Inferring the Labels by SDPM

The final label y_0 can be inferred in four ways. The first is the fast and easy way by directly outputting: $\hat{y}_0^{\text{avg}} = \hat{y}_0$, where \hat{y}_0 is the output of the trained network given the clean image x_0 . The second is based on the salient weight ψ_t over the time window T_i : $\hat{y}_0^{\text{sal}} = \frac{1}{N} \sum_{n=1}^N (\sum_{t=0}^{T_i < T} \hat{y}_0 \psi_t)$, where $\psi_t = 1 - (\frac{t}{T_i})^\nu$, $\nu > 1$ are gradually degraded coefficients. The third is based on the Markov chain inference starting at time T_i : $\hat{y}_0^{\text{infer}} = \frac{1}{N} \sum_{n=1}^N (\mathbf{IL}(d_i, T_i))$, where $d_i \in \mathbb{R}^{(0,1)}$, $T_i \in \{0, \dots, T\}$ and $\mathbf{IL}(\cdot)$ is the Algorithm 1. The last is the union of all the results: $\hat{y}_0^{\text{all}} = \hat{y}_0^{\text{avg}} \cup \hat{y}_0^{\text{sal}} \cup \hat{y}_0^{\text{infer}}$. Note that the second and third inferences are performed N times because of the randomness of noise. The average value of N time is used as the final result.

3 Experiments and Results

Datasets and Pre-processing: Two datasets were involved: 1) A private dataset, named **Infarct**, containing 195 AIS patient NCCT scans (5 mm) were included. Of 195 patients, 123 images were used for training while the remained 72 for testing. 2) Another private dataset comprising of 331 patients with acute intracranial hemorrhage confirmed by NCCT (2.5mm), called **Hemorrhage**, was

Algorithm 1 Inferencing Labels(IL) in Reverse Process

-
- 1: **Input:** image x_0 , **Parameters:** $d_i \in \mathbb{R}^{(0,1)}$, $T_i < T$
 - 2: **Initialization:** noised image $\hat{x}_{T_i} = x_{T_i}$ and noised label \hat{y}_{T_i} using (11)
 - 3: noise estimate $\hat{\varepsilon}_{T_i}$ using trained neural network
 - 4: **for** $t = T_i, \dots, 1$ **do**
 - 5: estimate \hat{x}_0, \hat{y}_0 using (11)
 - 6: **if** $t > 1$ **then**
 - 7: sampling $\varepsilon \sim \mathcal{N}(\mathbf{0}, \mathbf{I})$: estimate $\hat{x}_{t-1} = \sqrt{\alpha_{t-1}}\hat{x}_0 + \frac{\sqrt{\alpha_t}\gamma_{t-1}}{\sqrt{\gamma_t}}\hat{\varepsilon}_t + \frac{\beta_t\gamma_{t-1}}{\gamma_t}\varepsilon$
 - 8: and $\hat{y}_{t-1} = \sqrt{\alpha_{t-1}}\hat{y}_0 + \frac{\sqrt{\alpha_t}\gamma_{t-1}}{\sqrt{\gamma_t}}\hat{\varepsilon}_t + \frac{d_i\beta_t\gamma_{t-1}}{\gamma_t}\varepsilon$
 - 9: update next loop noise $\hat{\varepsilon}_{t-1}$ from \hat{x}_{t-1} using trained neural network
 - 10: **else if** $t = 1$ **then**
 - 11: estimate \hat{y}_0 using (11), $\hat{y}_0^{\text{final}} = \sqrt{\alpha_{t-1}}\hat{y}_0 + \frac{\sqrt{\alpha_t}\gamma_{t-1}}{\sqrt{\gamma_t}}\hat{\varepsilon}_t$
 - 12: **Output:** label estimate \hat{y}_0^{final}
-

also included patients with acute ICH confirmed by NCCT (2.5 mm thickness). Of 331 patient scans, 241 scans were used for training and validation, and 90 were used for testing.

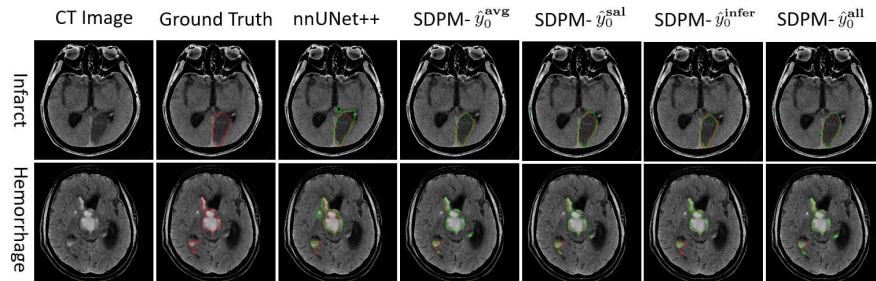
Hyper-parameters Settings: Online data augmentations was performed, including adding noise, rotations, scalings, inplane flipping, etc. Learning rate was reduced non-linearly from 1e-4 to 6e-5 with the Adam optimizer, where $lr = lr_{init} * (1 - i_c/i_{max})^{0.9} + lr_{min} * (i_c/i_{max})^{0.9}$, i_c is the current iteration and i_{max} is the maximum number of iteration. The variance schedule β_t is the sigmoid curve[17]. P2 Weighting coefficients during the training suggested in [18]. The repeated times are 100 and 50 for \hat{y}_0^{sal} and \hat{y}_0^{infer} in the inference process. Diffusion period T is 500 and the initial time $T_i = T/2$.

Evaluation Metrics: Three metrics[19] including Dice, Volume Correlation(VC) based on the Pearson product-moment correlation coefficient, and Volume Difference Percentages(VDP), were used to quantitatively assess the performance of the model prediction at a voxel level compared to manual contouring. Five other methods, including SegResNet, UNETR, SwinUNETR, nnUNet, nnUnet++, were also applied on the same three datasets. For fair comparisons, the best performance with the optimized parameters for each method was reported.

Results: A few segmentation examples are visualized in Fig.3. Quantitative results in Table.1 show SDPM with four inferences obtained the best performance on the whole with Dice, VC and VDP. The method 'CDPM w/o noise' is with the same neural network architecture but without diffusion process. In our private Infarct dataset, although SDPM w/o noise and \hat{y}_0^{all} have obtained nearly same dice of 0.4, SDPM- \hat{y}_0^{all} have better VC-0.619 and lower VDP-0.545. In hemorrhage dataset, the best performance by \hat{y}_0^{infer} is Dice-0.931, VC-0.985 and VDP-0.032. Additionally, Table.1 also suggested that our method was able to greatly reduce the VDP scores across three datasets.

Table 1. Quantitative performance on **Infarct** and **Hemorrhage**.

Datasets	Infarct			Hemorrhage		
Methods	Dice	VC	VDP	Dice	VC	VDP
SegResNet[20]	0.334	0.409	0.574	0.926	0.976	0.086
UNETR[21]	0.304	0.392	0.709	0.910	0.967	0.100
SwinUNETR[22]	0.366	0.455	0.656	0.908	0.965	0.101
nnUNet[23]	0.337	0.488	0.692	0.922	0.978	0.096
nnUNet++[24]	0.376	0.507	0.639	0.915	0.968	0.070
SegDiff[11]	0.389	0.482	0.658	0.927	0.976	0.066
MedSegDiff[10]	0.396	0.540	0.657	0.930	0.976	0.069
SDPM w/o noise[13]	0.400	0.557	0.633	0.927	0.961	0.074
SDPM- \hat{y}_0^{avg}	0.378	0.544	0.641	0.929	0.972	0.078
SDPM- \hat{y}_0^{infer}	0.374	0.531	0.652	0.931	0.985	0.067
SDPM- \hat{y}_0^{sal}	0.397	0.581	0.540	0.928	0.980	0.032
SDPM- \hat{y}_0^{all}	0.399	0.619	0.545	0.928	0.980	0.032

**Fig. 3.** Qualitative results for infarct and hemorrhage segmentations on two datasets

4 Discussion and Conclusion

A novel probabilistic SDPM is proposed to automatically segment stroke lesions of hemorrhage and infarct on NCCT, in order to alleviate the tedious manual contouring currently used in clinic [25]. The segmentation labels are output by SDPM in a fully probabilistic generative way. With the proposed several inference methods, the model was able to efficiently recover the lesion labels. Compared to the reference standard of manual contouring, quantitative evaluations demonstrate the efficacy of the proposed SDPM, outperforming several CNN and transformer based methods.

This study represents the first study to use a completely probabilistic inference model based on DPM to automatically segment infarct and hemorrhage on NCCT. Table.1 has shown the proposed SDPM with four inference methods obtained the start-of-the-art performance on two datasets. All the ablation studies in Table.1 revealed every inference method has its own strength, where salient weighting estimate \hat{y}_0^{all} reached the best VDP of 0.540 and 0.032, \hat{y}_0^{sal} obtained the best Dice in two infarct datasets. In the hemorrhage dataset, inference method \hat{y}_0^{infer} reached the best results of Dice and VC. Generally, the

inference of immediately outputting the labels performed worse than other three inference methods.

This study has several limitations. First, our datasets are limited. More training samples may further improve the segmentation accuracy and generalizability. Second, the final label inference is slightly influenced by stochastic factors. It is time-consuming to get an average prediction based on several inferences. Third, the predicted labels generated by different inference methods were simply averaged. More advanced label fusion techniques may improve the performance.

In conclusion, a synchronous image-label diffusion model by a LVM is proposed to segment stroke lesion of infarct and hemorrhage on NCCT. Experiments on three datasets demonstrate the efficacy of the proposed method, suggesting its potentials of being used for stroke lesion volume measurement.

References

1. A. Buckner, A. M. Boers, J. C. Bot, O. A. Berkhemer, H. F. Lingsma, A. J. Yoo, W. H. Van Zwam, R. J. Van Oostenbrugge, A. Van der Lugt, D. W. Dippel *et al.*, “Associations of ischemic lesion volume with functional outcome in patients with acute ischemic stroke: 24-hour versus 1-week imaging,” *Stroke*, vol. 48, no. 5, pp. 1233–1240, 2017.
2. J. M. Ospel, W. Qiu, B. K. Menon, A. Mayank, A. Demchuk, R. McTaggart, R. G. Nogueira, A. Y. Poppe, M. Jayaraman, B. Buck *et al.*, “Radiologic patterns of intracranial hemorrhage and clinical outcome after endovascular treatment in acute ischemic stroke: results from the escape-na1 trial,” *Radiology*, vol. 300, no. 2, pp. 402–409, 2021.
3. J. M. Ospel, B. K. Menon, W. Qiu, N. Kashani, A. Mayank, N. Singh, P. Cimflova, M. Marko, R. G. Nogueira, R. A. McTaggart *et al.*, “A detailed analysis of infarct patterns and volumes at 24-hour noncontrast ct and diffusion-weighted mri in acute ischemic stroke due to large vessel occlusion: results from the escape-na1 trial,” *Radiology*, vol. 300, no. 1, pp. 152–159, 2021.
4. A. Dobshik, S. Verbitskiy, I. Pestunov, K. Sherman, Y. N. Sinyavskiy, A. Tulupov, and V. Berikov, “Acute ischemic stroke lesion segmentation in non-contrast ct images using 3d convolutional neural networks,” *arXiv:2301.06793*, 2023.
5. R. Gauriau, B. C. Bizzo, D. S. Comeau, J. M. Hillis, C. P. Bridge, J. K. Chin, J. Pawar, A. Pourvaziri, I. Sestic, E. Sharaf *et al.*, “Head ct deep learning model is highly accurate for early infarct estimation,” *Scientific Reports*, vol. 13, no. 1, p. 189, 2023.
6. K. Liang, K. Han, X. Li, X. Cheng, Y. Li, Y. Wang, and Y. Yu, “Symmetry-enhanced attention network for acute ischemic infarct segmentation with non-contrast ct images,” in *Medical Image Computing and Computer Assisted Intervention–MICCAI 2021: 24th International Conference, Strasbourg, France, September 27–October 1, 2021, Proceedings, Part VII 24*. Springer, 2021, pp. 432–441.
7. L. Liu, L. Kurgan, F.-X. Wu, and J. Wang, “Attention convolutional neural network for accurate segmentation and quantification of lesions in ischemic stroke disease,” *Medical Image Analysis*, vol. 65, p. 101791, 2020.
8. J. Sohl-Dickstein, E. Weiss, N. Maheswaranathan, and S. Ganguli, “Deep unsupervised learning using nonequilibrium thermodynamics,” in *International Conference on Machine Learning*. PMLR, 2015, pp. 2256–2265.

9. D. Baranchuk, I. Rubachev, A. Voynov, V. Khrukov, and A. Babenko, "Label-efficient semantic segmentation with diffusion models," *arXiv:2112.03126*, 2021.
10. J. Wu, H. Fang, Y. Zhang, Y. Yang, and Y. Xu, "Medsegdiff: Medical image segmentation with diffusion probabilistic model," *arXiv:2211.00611*, 2022.
11. T. Amit, E. Nachmani, T. Shaharbany, and L. Wolf, "Segdiff: Image segmentation with diffusion probabilistic models," *arXiv:2112.00390*, 2021.
12. Y. Song and S. Ermon, "Generative modeling by estimating gradients of the data distribution," *Advances in neural information processing systems*, vol. 32, 2019.
13. J. Ho, A. Jain, and P. Abbeel, "Denoising diffusion probabilistic models," *Advances in Neural Information Processing Systems*, vol. 33, pp. 6840–6851, 2020.
14. S. Sommer, "Anisotropic distributions on manifolds: Template estimation and most probable paths," in *Information Processing in Medical Imaging: 24th International Conference, IPMI 2015, Sabhal Mor Ostaig, Isle of Skye, UK, June 28-July 3, 2015, Proceedings 24*. Springer, 2015, pp. 193–204.
15. R. Lopez, J. Regier, M. I. Jordan, and N. Yosef, "Information constraints on auto-encoding variational bayes," *Advances in neural information processing systems*, vol. 31, 2018.
16. A. Voynov, K. Aberman, and D. Cohen-Or, "Sketch-guided text-to-image diffusion models," *arXiv:2211.13752*, 2022.
17. A. Q. Nichol and P. Dhariwal, "Improved denoising diffusion probabilistic models," in *International Conference on Machine Learning*. PMLR, 2021, pp. 8162–8171.
18. J. Choi, J. Lee, C. Shin, S. Kim, H. Kim, and S. Yoon, "Perception prioritized training of diffusion models," in *Proceedings of the IEEE/CVF Conference on Computer Vision and Pattern Recognition*, 2022, pp. 11 472–11 481.
19. A. A. Taha and A. Hanbury, "Metrics for evaluating 3d medical image segmentation: analysis, selection, and tool," *BMC medical imaging*, vol. 15, no. 1, pp. 1–28, 2015.
20. A. Myronenko, "3d mri brain tumor segmentation using autoencoder regularization," in *Brainlesion: Glioma, Multiple Sclerosis, Stroke and Traumatic Brain Injuries: 4th International Workshop, BrainLes 2018, Held in Conjunction with MICCAI 2018, Granada, Spain, September 16, 2018, Revised Selected Papers, Part II 4*. Springer, 2019, pp. 311–320.
21. A. Hatamizadeh, Y. Tang, V. Nath, D. Yang, A. Myronenko, B. Landman, H. R. Roth, and D. Xu, "Unetr: Transformers for 3d medical image segmentation," in *Proceedings of the IEEE/CVF winter conference on applications of computer vision*, 2022, pp. 574–584.
22. A. Hatamizadeh, V. Nath, Y. Tang, D. Yang, H. R. Roth, and D. Xu, "Swin unetr: Swin transformers for semantic segmentation of brain tumors in mri images," in *Brainlesion: Glioma, Multiple Sclerosis, Stroke and Traumatic Brain Injuries: 7th International Workshop, BrainLes 2021, Held in Conjunction with MICCAI 2021, Virtual Event, September 27, 2021, Revised Selected Papers, Part I*. Springer, 2022, pp. 272–284.
23. F. Isensee, P. F. Jaeger, S. A. Kohl, J. Petersen, and K. H. Maier-Hein, "nnu-net: a self-configuring method for deep learning-based biomedical image segmentation," *Nature methods*, vol. 18, no. 2, pp. 203–211, 2021.
24. Z. Zhou, M. M. Rahman Siddiquee, N. Tajbakhsh, and J. Liang, "Unet++: A nested u-net architecture for medical image segmentation," in *Deep Learning in Medical Image Analysis and Multimodal Learning for Clinical Decision Support: 4th International Workshop, DLMIA 2018, and 8th International Workshop, ML-CDS 2018, Held in Conjunction with MICCAI 2018, Granada, Spain, September 20, 2018, Proceedings 4*. Springer, 2018, pp. 3–11.

25. N. Samuels, K. C. Compagne, N. A. van der Ende, V. Chalos, P. R. Konduri, P. J. van Doormaal, W. H. van Zwam, C. B. Majoie, H. A. Marquering, B. Roozenbeek *et al.*, "Infarct volume after ischemic stroke as a mediator of the effect of endovascular thrombectomy on early postprocedural neurologic deficit," *Journal of Stroke and Cerebrovascular Diseases*, vol. 32, no. 2, p. 106906, 2023.

This figure "fig31.png" is available in "png" format from:

<http://arxiv.org/ps/2307.01740v2>